Electronic Supplementary Material (ESI) for Journal of Materials Chemistry A.

Supplementary Information

Scalable Preparation of Hierarchical Porous Activated Carbon/graphene composite for High-Performance Supercapacitors

Yilun Huang,[a,b,c] Yunkai Shi,[a,b,c] Qianming Gong,*[a,b,c] Mouyi Weng,[d] Yuyao Li,[a,b,c] Jianning Gan,[a,b,c] Dazhi Wang,[e] Yang Shao,[a,c] Ming Zhao,[a,c] Daming Zhuang,[a,b,c] Ji Liang,[f] Feng Pan,*[d] Hongwei Zhu [a,b,c] and Cewen Nan [a,b,c]

[a.] School of Materials Science and Engineering, Tsinghua University, Beijing 100084, P.R. China. Email: gongqianming@mail.tsinghua.edu.cn

[b.] State Key Laboratory of New Ceramics and Fine Processing, Tsinghua University, Beijing 100084, P. R. China.

[c.] Key Laboratory for Advanced Materials Processing Technology, Ministry of Education, Beijing 100084, P. R. China.

[d.] School of Advanced Materials, Shenzhen Graduate School, Peking University, Shenzhen 518055, P.R. China. Email: panfeng@pkusz.edu.cn

[e.] Beijing HCC Energy Technology Co., Ltd, Beijing 100085, P. R. China.

[f.] Department of Mechanical Engineering, Tsinghua University, Beijing 100084, P. R. China.

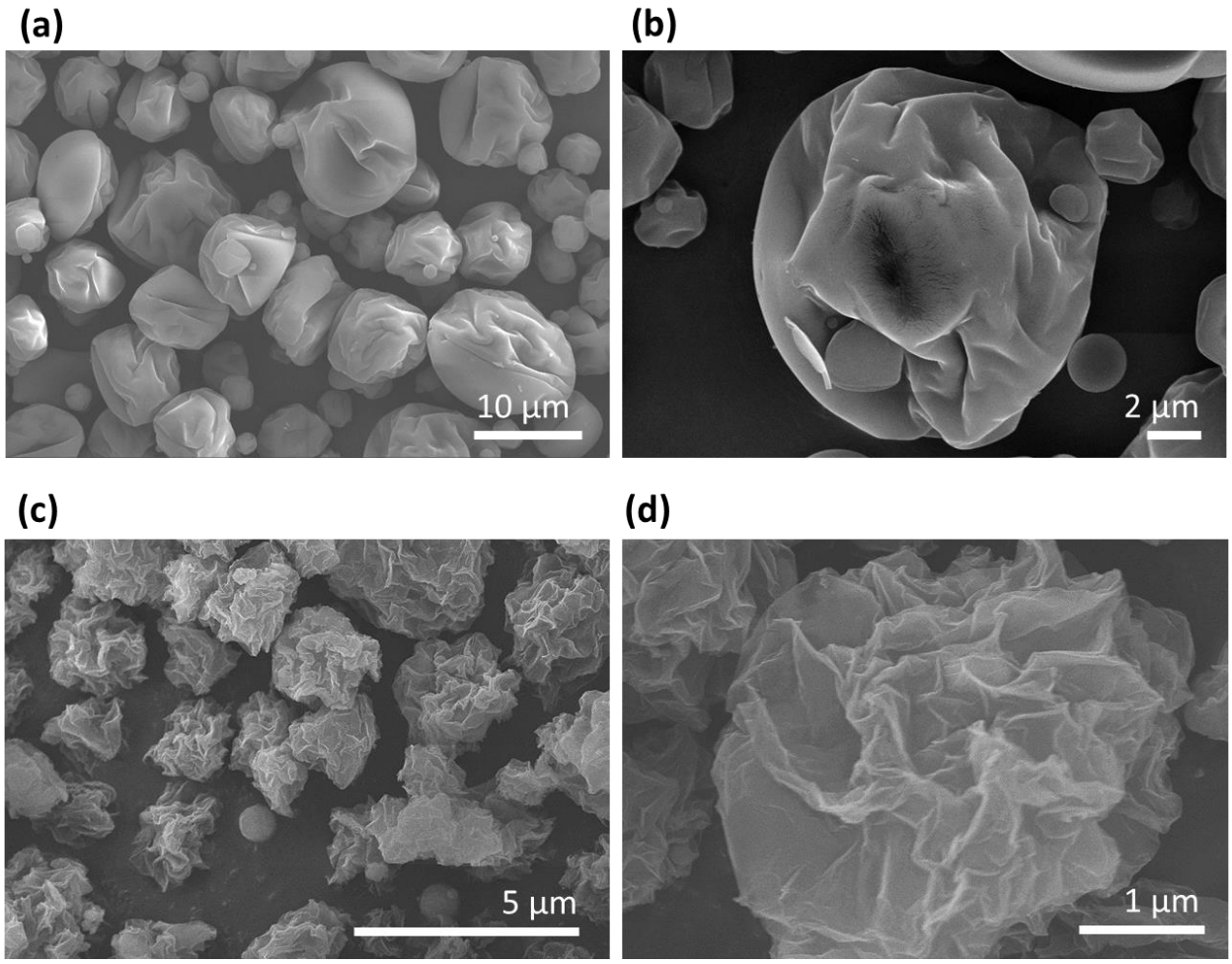

Figure S1. SEM images of (a, b) 10 wt. % GO mixed with maltodextrin powders (GMP-10) and (c, d) pure GO powders prepared by spray-drying method. The pure GO powdery particles are flower-like with many wrinkles, and the 10 wt. % GO/maltodextrin particles have more wrinkles in their surfaces than 5 wt. % GO/maltodextrin particles, which indicates that the GO forms the wrinkled shell to cover maltodextrin.

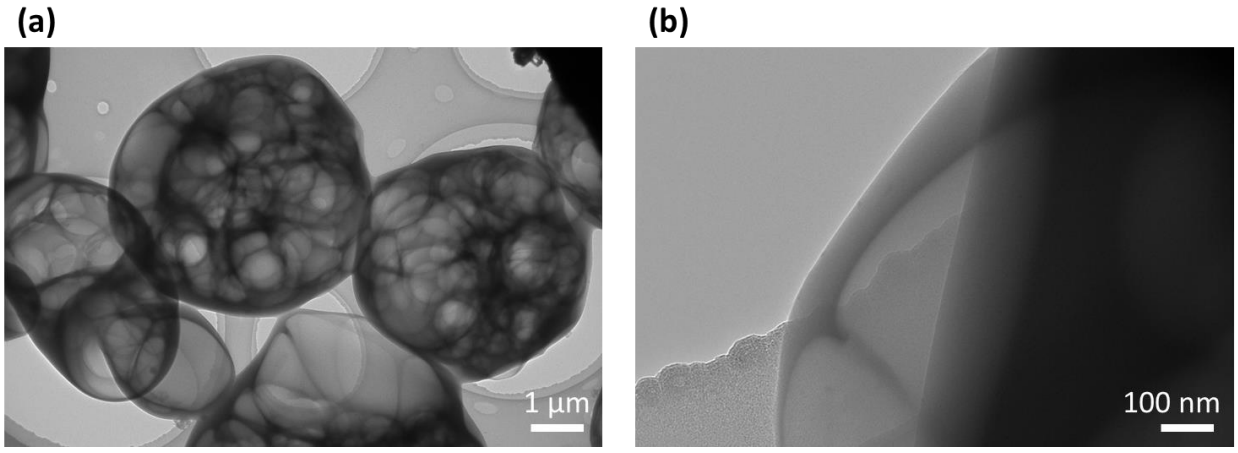

Figure S2. TEM images of GMP-10.

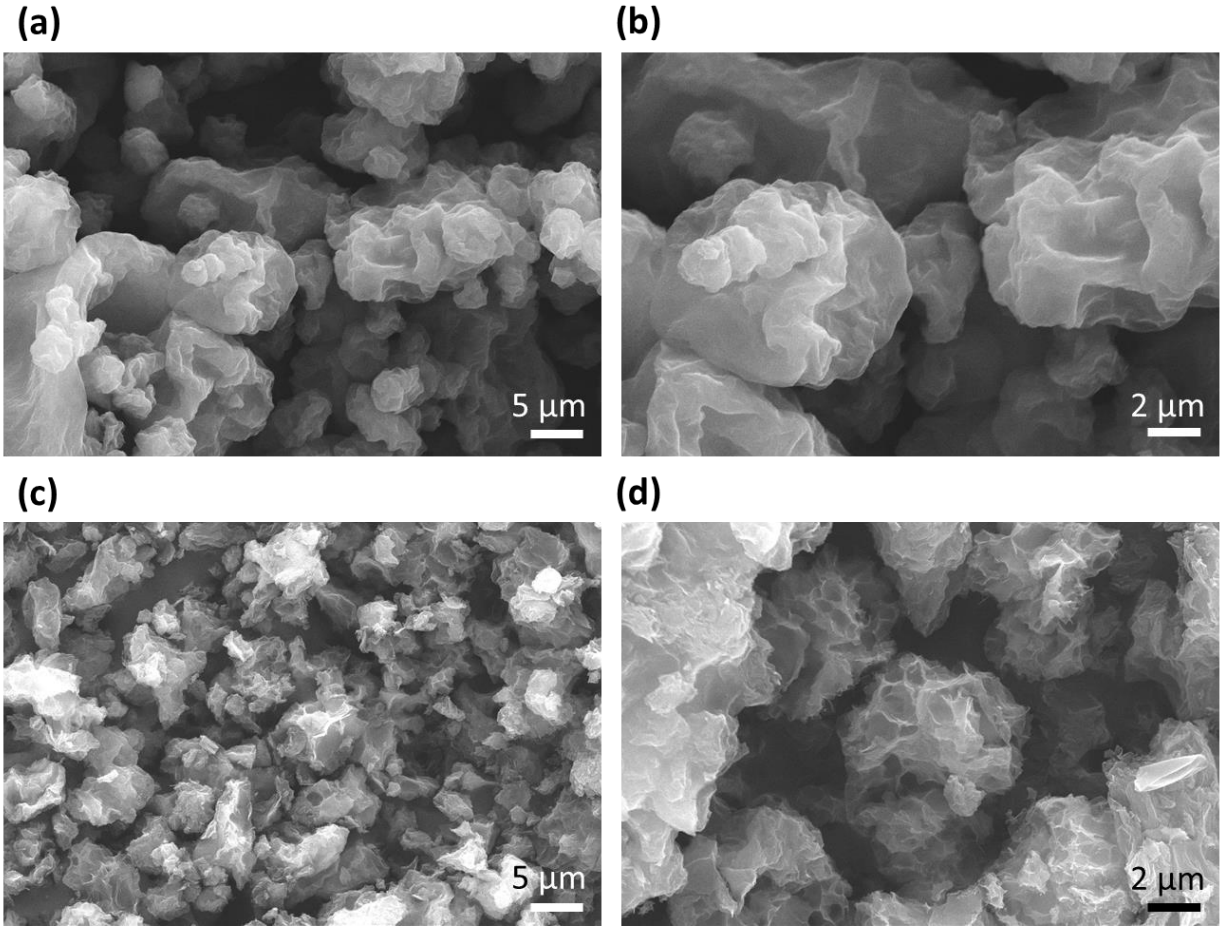

Figure S3. SEM images of (a) (b) c-GMP-10 and (c) (d) a-GMP-10.

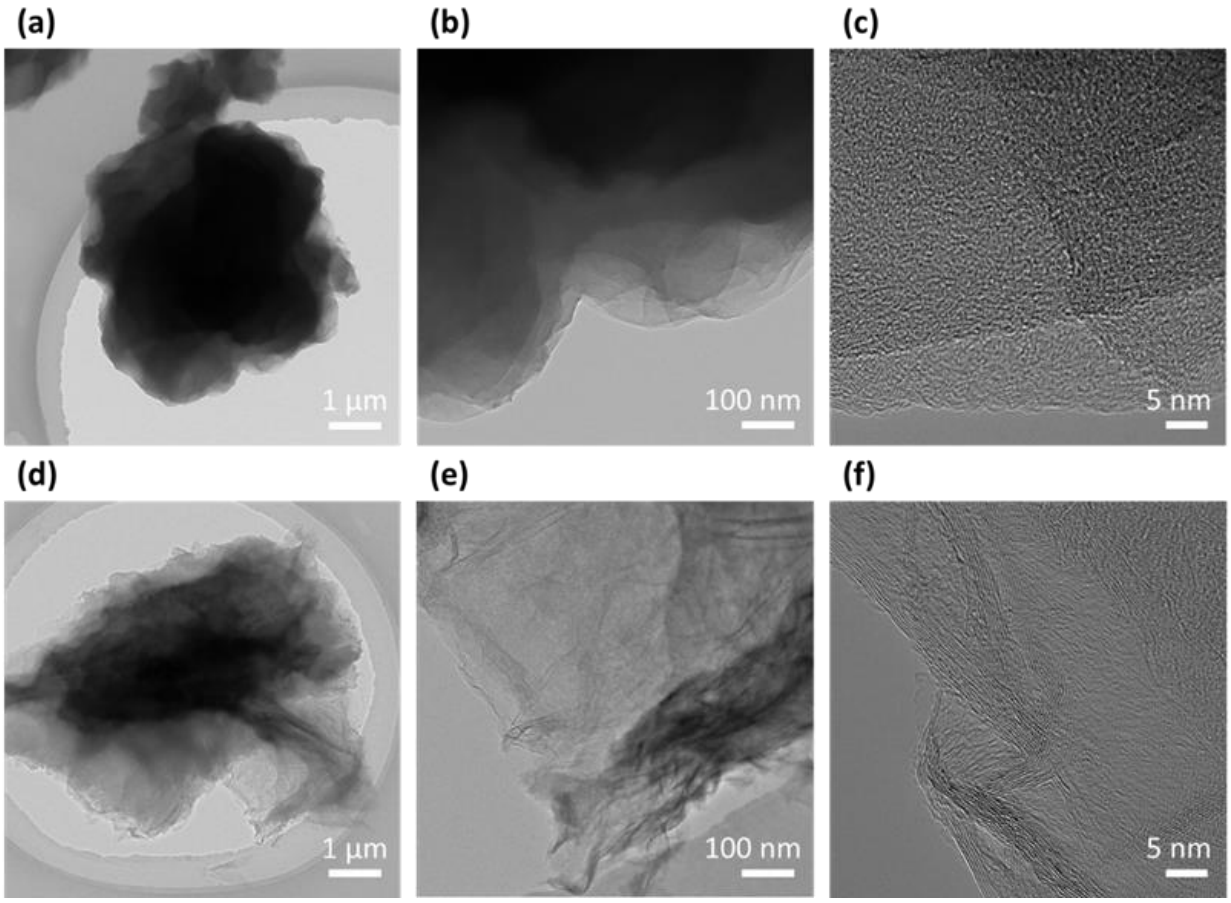

Figure S4. TEM images of (a, b) GMP-10, (c, d, e) c-GMP-10 and (f, g, h) a-GMP-10.

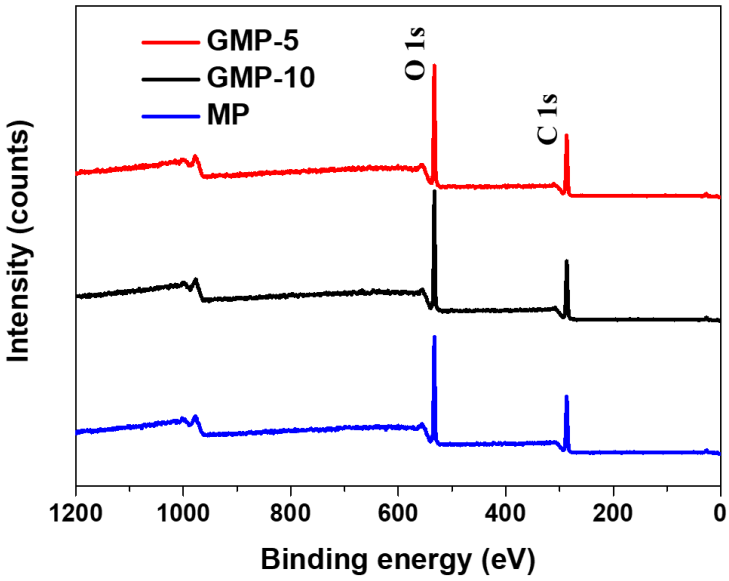

Figure S5. XPS survey spectra of raw materials (GMP-5, GMP-10 and MP).

Table S1. The element variation of the samples from XPS results.

Sample	**Atomic Concentration (%)**			
	C	O	S	Total
GMP-5	60.14	39.34	0.14	100
GMP-10	59.32	40.48	0.20	100
MP	59.42	40.58	-	100
a-GMP-5	94.23	5.77	-	100
a-GMP-10	96.49	3.51	-	100
a-MP	95.13	4.87	-	100

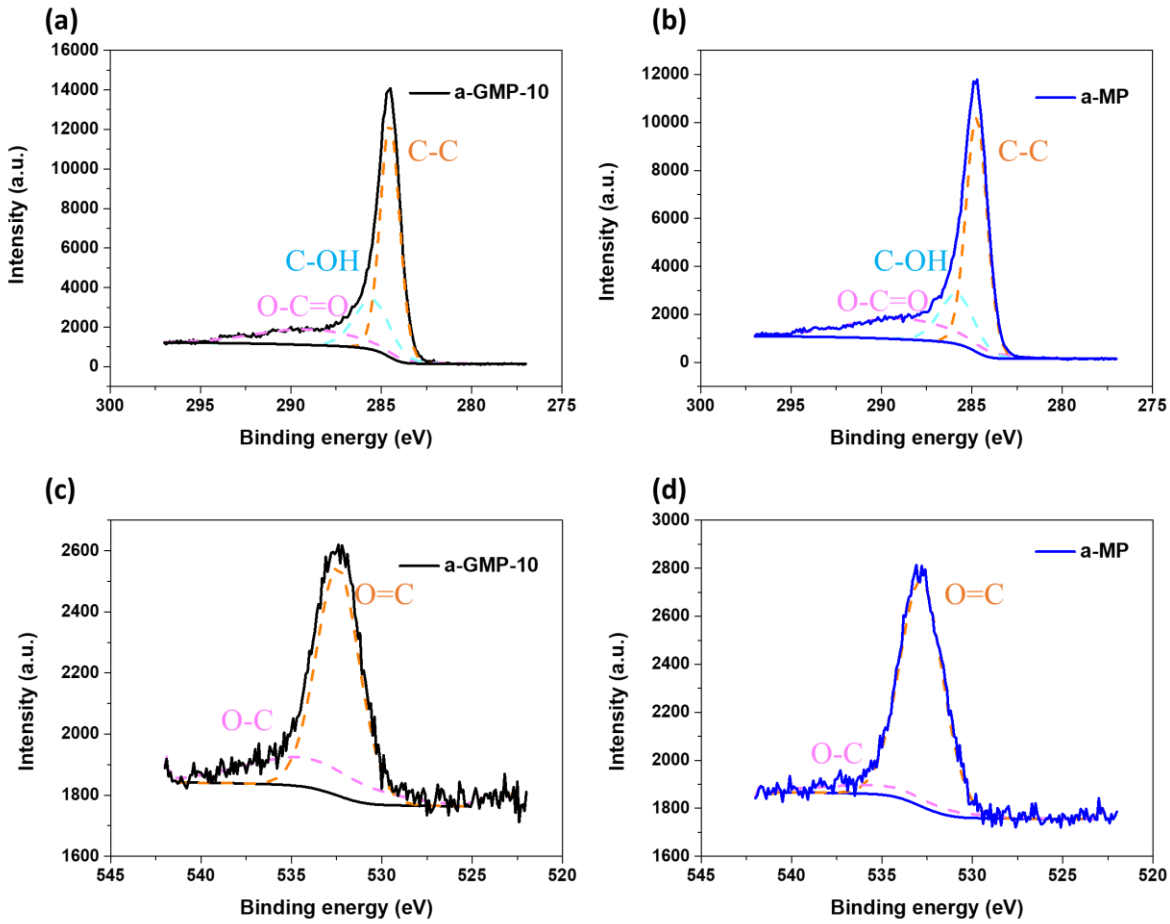

Figure S6. High resolution (a, b) C 1s and (c, d) O 1s XPS spectra of a-GMP-10 and a-MP samples.

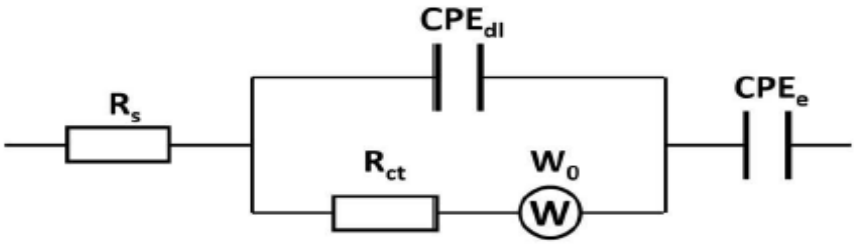

Figure S7. The equivalent circuit model used in EIS tests.[1]

The experimental results (**Figure 4b**) can be well fitted with the provided circuit. In the high frequency region of Nyquist plot, R_S can be obtained by intersection of the curve and the real axis, including the interfacial contact resistance between electroactive material and current collector, the resistance of the electrolyte and inherent resistance of current collector. And the diameter of the semicircle corresponds to the charge transfer resistance (R_{ct}) which is associated with the porous structure of the electrode. What's more, constant phase elements (CPE_{dl}) can also be represented by semicircles due to double layer behavior. In the middle frequency region, the inclined curve of approximately 45 °corresponds to the Warburg impedance (W_0), indicating the ionic diffusion in the electrodes. In the low frequency region, the curve approximately perpendicular to the real axis shows a nearly ideal electrochemical capacitive behavior of the electrodes, and another CPE_e was added to the circuit due to the possible existing of pseudo-capacitive behavior.

Table S2. Summarized resistances of the electrodes obtained by EIS.

Samples	ESR (R_Ω)	R_{ct}	R_{total}*
a-GMP-5	0.53	0.21	0.74
a-GMP-10	0.40	0.23	0.63
a-MP	0.56	0.50	1.06

* $R_{total}=R_\Omega+R_{ct}$

Table S3. Capacitive performance of the samples in this work and other selected carbon materials in references with aqueous electrolytes.

Materials	Electrolyte	Charge/discharge current density (A g^{-1}) or scan rate (mV s^{-1})	Specific capacitance (F g^{-1})	Reference
Hierarchical porous graphene network	KOH	1 A g^{-1}	306	1
Porous graphene/activated carbon composite	KOH	1 A g^{-1}	306	2
Activated graphene aerogel	KOH	0.2 A g^{-1}	204	3
Graphene activated carbon	KOH	0.1 A g^{-1}	122	4
3D hierarchical porous carbon material	Na_2SO_4	0.2 mV s^{-1}	294	5
N-doped hierarchical porous carbon/graphene	KOH	1 A g^{-1}	318	6
Carbon aerogels	KOH	0.5 A g^{-1}	302	7
Porous carbon	KOH	1 A g^{-1}	272	8
Core-shell hierarchical porous graphene-covered activated carbon	KOH	0.2 A g^{-1}	406	This work
		1 A g^{-1}	299	

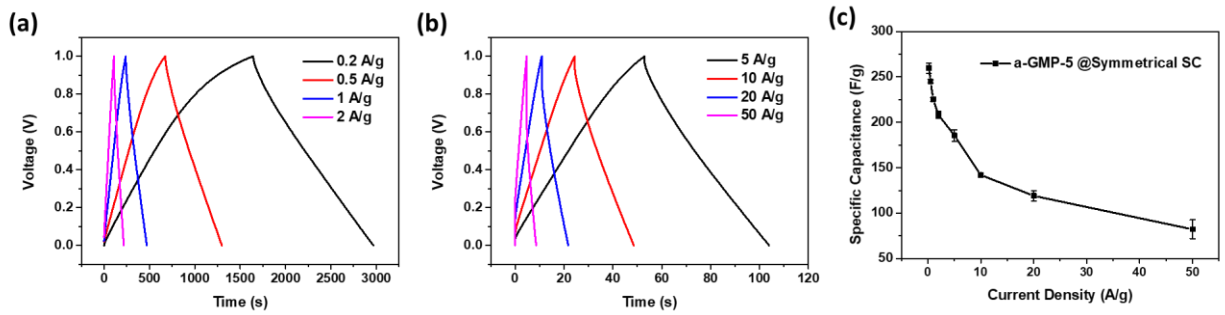

Figure S8. (a) (b) GCD curves for a-GMP-5 in two-electrode cell obtained at different current densities from 0.2 to 50 A g^{-1}. (c) Specific capacitances of a-GMP-5 at different current densities from 0.2 to 50A g^{-1}, which were measured from GCD curves.

In order to calculate the energy density and power density, a-GMP-5 was also examined as an electrode material in two-electrode supercapacitor cells. The two-electrode cell was charged and discharged at different current density from 0.2 to 50 A g^{-1}. **Figure 8a** and **8b** shows the GCD curves of the cell. The specific capacitance (C_s in F g^{-1}, showing in **Figure 8c**) was calculated by equation (1) based on the GCD experimental data, where I is the discharge current (A), m is the total mass of two electrodes (g), Δt is the discharge time (s), and ΔV is the discharge potential window (V). The energy density (E in Wh kg^{-1}) and power density (P in W kg^{-1}) were calculated by equation (2) and equation (3).

$$C_s = \frac{4I \times \Delta t}{\Delta V \times m} \quad (1)$$

$$\mathrm{E} = \frac{C_S \times (\Delta V)^2}{2 \times 3.6} \quad (2)$$

$$\mathrm{P} = \frac{E}{\Delta t} \times 3600 \quad (3)$$

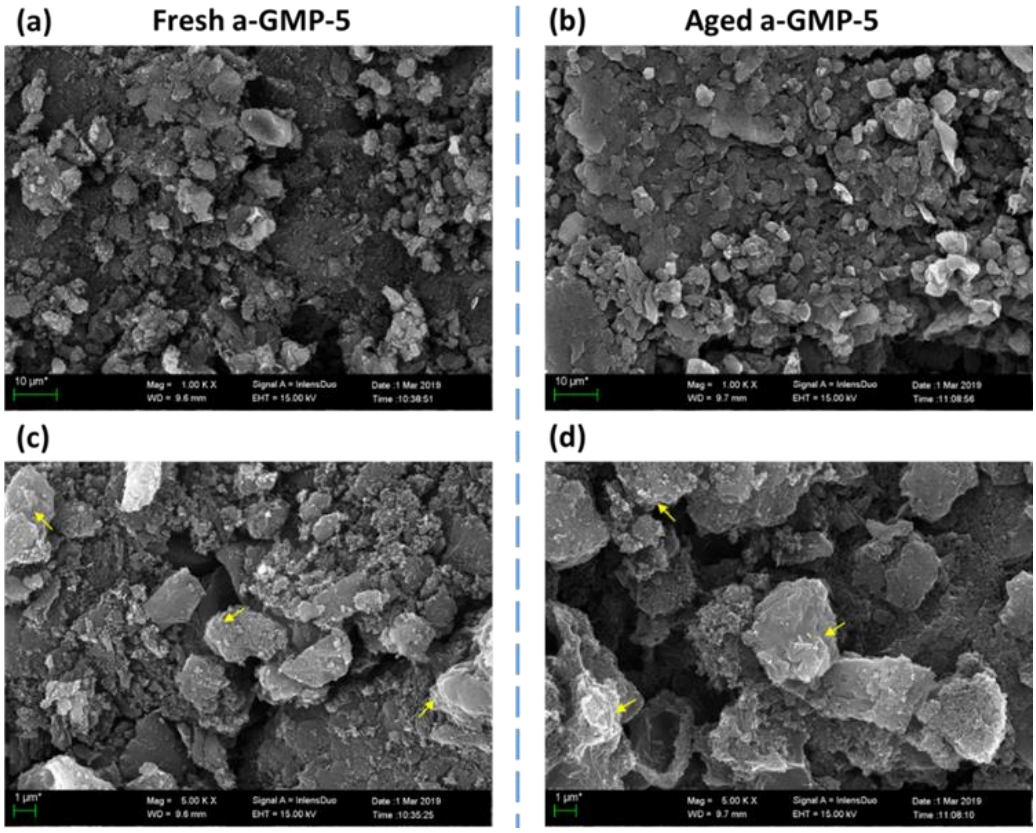

Figure S9. SEM images of (a, c) fresh a-GMP-5 and (b, d) aged a-GMP-5.

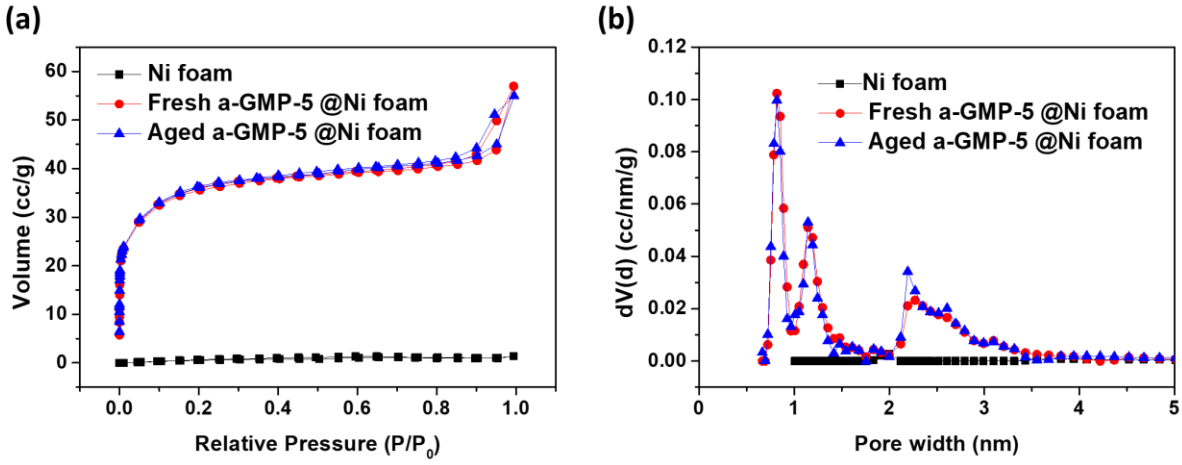

Figure S10. (a) N_2 adsorption/desorption isotherms and (b) pore-size distributions of a-GMP-5 and aged a-GMP-5 @Ni foam electrodes and pure nickel foam current collector.

Table S4. Specific surface areas and pore volume of the samples and corresponding weight for BET tests.

Samples	SSA[a] (m^2/g)	Pore volume[b] (cc/g)	Sample weight (mg)	Active material weight[c] (mg)
Ni foam	3.1	2.08	53.6	/
Fresh a-GMP-5 @Ni foam	107.5	8.81	42.9	3.66
Aged a-GMP-5 @ Ni foam	116.1	8.50	43.2	3.90

[a] Calculated from BET results.

[b] Total pore volume for pores with diameter less than 343.85 nm at $P/P_0 = 0.994402$.

[c] Active material weight = (Sample weight − Ni foam weight) * Ratio of active material

Figure S9 shows the variation of the microstructure of fresh a-GMP-5 and aged a-GMP-5. There is no distinct difference between the fresh and the aged a-GMP-5 at low magnification (**Figure S9a** and **S9b**). The wrinkled structures of rGO shell on the surface of a-GMP-5 marked by arrows remain unchanged after cycling (**Figure S9c** and **S9d**). While in the meantime, we also know that it is not reasonable to draw a conclusion just according to some specific fields of view in SEM observations. Comparatively, statistic BET analyses would be more valuable in evaluating the variation of the pore structure of a-GMP-5 before and after cycling tests. Specifically, **Figure S10** shows N_2 adsorption/desorption isotherms and pore-size distributions of the fresh and aged integrated electrodes (being denoted as a-GMP-5 @Ni foam) comparing with pure nickel foam current collector. It can be seen that nickel foam current collector has few pores and a low specific surface area (SSA) of 3.1 $m^2 g^{-1}$, which can be neglected compared with the high SSA of a-GMP-5. Similarly, the effect of nickel foam on the pore size distribution

(PSD) of the integrated electrode is negligible as well (**Figure S10b**), so we just focused on the comparison between the curves of the fresh/aged integrated electrodes. The PSD results show that both fresh and aged a-GMP-5 have intensive micropores with the size of 0.85 nm and 1.36 nm. They also exhibit similar broad peaks ranging from 2 to 4 nm, which indicates there are some mesopores in a-GMP-5. Based on the quantitative results in **Table S4**, we found that neither the pore volume nor the SSA of fresh a-GMP-5 @Ni foam electrode decreased after cycling tests. So herein, the deduction that graphene conduced to stabilize the microstructure, especially the pore structure during cycling tests is reasonable to some extent.

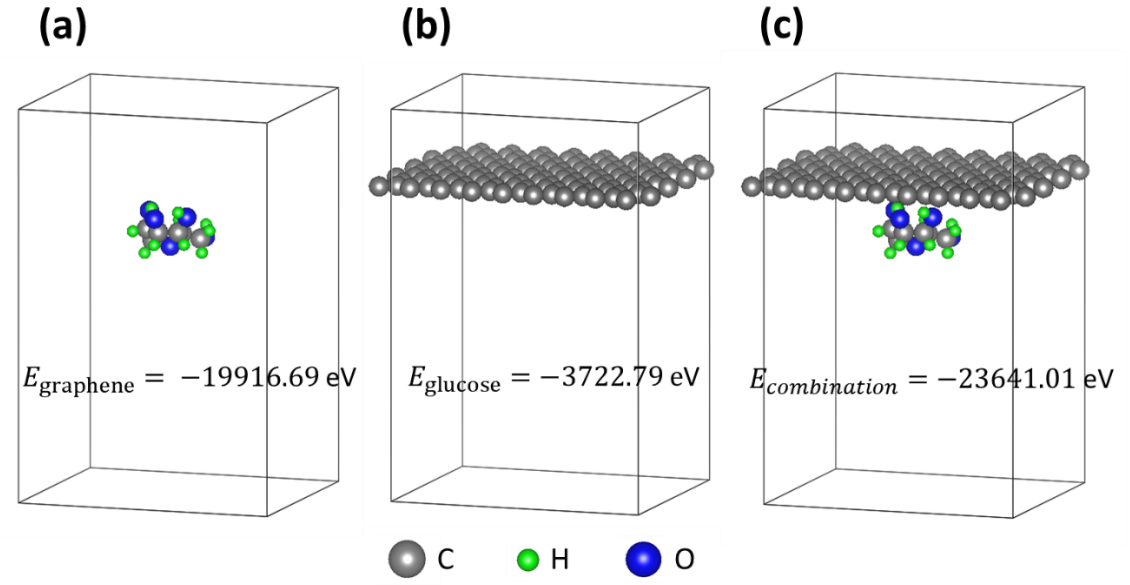

Figure S11. The structure of (a) glucose, (b) graphene, and (c) graphene combined with maltose, with a vacuum layer in its *b* direction. The calculated adsorption energy $E_{adsorption} = E_{combination} - E_{\text{molecular}} - E_{\text{graphene}} = -1.528$ eV indicates that the combination of glucose and the graphene layer is more energetically favourable than the separated structures.

Table S5. The atomic concentration of the samples from XPS results.

Sample	Atomic Concentration (%)			
	C	O	S	Total
GO	64.33	33.95	1.72	100
MP	59.42	40.58	-	100
GMP-10	59.32	40.48	0.20	100
o-GMP-10	59.63	40.31	0.06	100

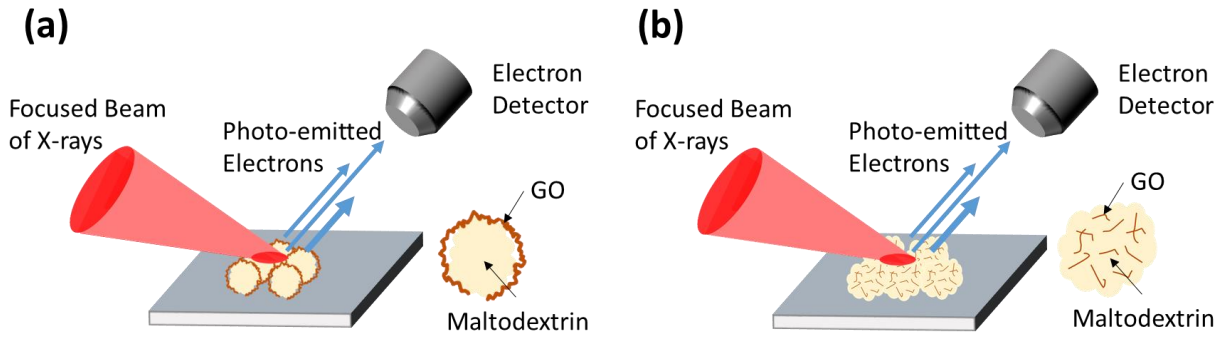

Figure S12. Schematic illustration of the XPS tests of (a) GMP-10 and (b) o-GMP-10.

Table S6. The amounts of active material loaded in different electrodes.

Samples	Amount of the active material (mg)	Average (mg)
a-GMP-5-1#	3.72	3.77
a-GMP-5-2#	3.51	
a-GMP-5-3#	4.07	
a-GMP-10-1#	3.08	3.93
a-GMP-10-2#	5.11	
a-GMP-10-3#	3.59	
a-MP-1#	3.70	3.08
a-MP-2#	3.22	
a-MP-3#	2.32	
Commercial AC-1#	5.45	4.03
Commercial AC-2#	2.82	
Commercial AC-3#	3.82	

References:

1. Z. N. Li, S. Gadipelli, Y. C. Yang and Z. X. Guo, *Small*, 2017, **13**, 1702474.
2. Z. Chao, X. Zhou, H. Cao, G. Wang and Z. Liu, *J Power Sources*, 2014, **258**, 290-296.
3. X. X. Sun, P. Cheng, H. J. Wang, H. Xu, L. Q. Dang, Z. H. Liu and Z. B. Lei, *Carbon*, 2015, **92**, 1-10.
4. Y. Chen, X. Zhang, H. Zhang, X. Sun, D. Zhang and Y. Ma, *Rsc Advances*, 2012, **2**, 7747-7753.
5. W. Qian, J. Yan, Y. Wang, W. Tong, M. Zhang, X. Jing and Z. J. C. Fan, *Carbon*, 2014, **67**, 119-127.
6. Y. Y. Yin, R. Y. Li, Z. J. Li, J. K. Liu, Z. G. Gu and G. L. Wang, *Electrochim Acta*, 2014, **125**, 330-337.
7. G. Q. Zu, J. Shen, L. P. Zou, F. Wang, X. D. Wang, Y. W. Zhang and X. D. Yao, *Carbon*, 2016, **99**, 203-211.
8. Y. Zhong, T. Shi, Y. Huang, S. Cheng, G. Liao and Z. Tang, *Electrochim Acta*, 2018, **269**, 676-685.